

Exploration of SMEFT Interpretation of $t\bar{t}t\bar{t}$ Production

University of Victoria
Physics and Astronomy Co-op Program:
Summer 2022, Work Term I

By

Kyran Klazek-Schryer
V00941471
University of Victoria, Dept. of Physics & Astronomy

Performed at:
University of British Columbia, Vancouver, Canada
and
CERN (European Laboratory for Particle Physics), Geneva, Switzerland

Supervisor(s): Dr. Abhishek Sharma, Dr. Alison Lister, Dr. Colin Gay
University of British Columbia, Dept. of Physics & Astronomy / CERN, ATLAS Collaboration

Exploration of SMEFT Interpretation of $t\bar{t}t\bar{t}$ Production

Kyran Klazek-Schryer

University of Victoria / ATLAS Collaboration

Supervisors: Abhishek Sharma, Alison Lister, Colin Gay

University of British Columbia / ATLAS Collaboration

August 19 2022

Abstract

As part of the CERN Summer Student Programme 2022, I worked with the ATLAS Detector Collaboration. My research was affiliated with the ‘Non Resonant BSM in 4-tops’ group, working on $t\bar{t}t\bar{t}$ cross section measurement, and new physics BSM searches using $t\bar{t}t\bar{t}$ (2 same sign lepton/3+ lepton final states) production. My specific analysis focused on the effects of SMEFT parameter introduction on the yield and shape of the nominal 4-top signal. Different center-of-mass (CM) frame variables were explored to determine which ones provided the best shape difference from the nominal signal, to provide difference on which to train future neural networks. Yield and shape comparison plots were created for many CM variables, distinguishing the nominal signal from the EFT-varied signal. The variables that were found to have the largest shape differences were those involving top quark momentum: ΣP_{top} , $min P_{top}$ and $max P_{top}$. Future continuations of this analysis could include implementing these variables into the training of a Neural Network, namely GNNs.

Contents

1	Introduction	2
1.1	What is Standard Model EFT?	2
1.2	Description of 4-top $t\bar{t}t\bar{t}$ production	3
1.3	Why is $t\bar{t}t\bar{t}$ useful for EFT interpretations?	3
2	Existing Analysis / Tools	4
2.1	TRExFitter	4
2.1.1	EFTRExFitter	5
2.2	Recursive Jigsaw Reconstruction, RJR	5
2.3	Boosted Decision Trees, BDT	6
2.4	mva-trainer & Graph Neural Networks, GNNs	6
3	Procedure / My Contributions	7
3.1	Working with EFTRExFitter	7
3.1.1	Config File Differences	7
3.1.2	Higgs Oblique Difficulties	10
3.2	Working with mva-trainer	11
4	Results / Discussion	11
4.1	Findings & Results	11
4.2	Future Directions / Discussion	11

A Appendix: Negative Log-Likelihood Plots	13
B Appendix: Rate and Shape Comparison Plots	15
B.1 Signal Region(s)	15
B.2 Control Regions	18
B.3 Verification Regions	18
B.4 Recursive Jigsaw Regions	18
C Input Variables for \hat{H} and Nominal $t\bar{t}t\bar{t}$ Comparison	23

1 Introduction

As part of the CERN Summer Student Programme 2022, I took part in High Energy Physics (HEP) research during the summer. My project was within the ATLAS Detector collaboration, one of the collaborations associated with the particle detectors around the Large Hadron Collider (LHC) at CERN in Geneva, Switzerland. I worked under the supervision of Abhishek Sharma, a postdoc at the University of British Columbia, spending half my summer working at UBC and the other half working remotely from the CERN campus in Geneva, along with fellow students from around the world partaking in the Summer Programme.

My research was affiliated with the analysis being conducted by the ‘Search for Non-Resonant BSM in Four-Tops’ Working Group, which is an ATLAS Collaboration research group working on the measurement of 4-top-quark ($t\bar{t}t\bar{t}$) production, as well as the search for new physics Beyond the Standard Model (BSM) with four top quark events. Using ATLAS detector data from the LHC’s Run 2 (2015-2018) with a collision center-of-mass energy of $\sqrt{s} = 13\text{TeV}$, $t\bar{t}t\bar{t}$ events are selected if they contain a same-sign lepton pair, or three or more leptons (electrons and muons). Jet multiplicity, flavour and kinematics are also used to further distinguish the signal [1]. At the time of my contributions, the analysis was not unblinded to real data, and was working with Monte Carlo (MC) simulations of four-top production. My research specifically focused on the BSM aspect of the analysis, exploring new-physics effects in the context of Standard Model Effective Field Theory (SMEFT). I explored the comparison of yield and shape differences in the signal distribution caused by the activation of different EFT parameters, using different regions of the phase space.

1.1 What is Standard Model EFT?

Standard Model Effective Field Theory (SMEFT) is a model-independent framework for characterizing deviations from the Standard Model (SM) predictions in experiments. This EFT provides a structure to some of the possible extensions of the SM, which are integral in the search for physics Beyond the Standard Model (BSM). In SMEFT, it is assumed that the quantum numbers of SM particles are correctly assigned, which gives the structure of the terms in the SM Lagrangian with dimension 4 or less, while knowing that it is incomplete. The effective field theory allows for higher order interactions between known particles while still respecting Standard Model symmetries. In this regard, SMEFT essentially modifies and alters the couplings between existing SM particles in a minimal way, such that evidence for BSM physics is present and accounted for, but not constrained to a specific BSM model with specific new particles. The possible strengths of the higher order interactions are constrained by observed experiment data. Due to extreme CP violation with (most) odd-dimension operators, standard EFT analyses look at dimension-6 operators. Of the 2499 possible dimension-6 operators in the SMEFT Lagrangian, many are disregarded due to simplifying assumptions about flavour structure and symmetries [8].

The SMEFT Lagrangian takes the form:

$$\mathcal{L}_{SMEFT} = \mathcal{L}_{SM} + \sum \frac{c_i}{\Lambda^2} \mathcal{O}_i \quad (1)$$

where \mathcal{O} are the operators, c are the *Wilson coefficients* determining the strength of its related operator, and Λ is the energy level which is being probed (in our case $\Lambda = 1\text{TeV}$). This is a low enough energy that the higher dimension-8 operators, at the order of $1/\Lambda^4$, can be neglected.

Our analysis looks at five Wilson coefficients of SMEFT operators in the Warsaw basis: c_{QQ}^1 , c_{Qt}^1 , c_{Qt}^8 , c_{tt}^1 , and \hat{H} —the Higgs Oblique Parameter. The subscript represents the particle on either side of the interaction, with Q being a left-handed heavy quark doublet and t a right-handed top-type quark singlet [4]. The superscript represents a difference in spin structure between the input and output of the interaction. The Higgs Oblique parameter is the only dimension-6 operator that modifies the Higgs boson propagator [9].

The goal of EFT analyses is to use precision measurements of, in our case top and Higgs production, to constrain the possible values for the various Wilson coefficients. This is difficult to do methodically and systematically as the behaviours of the operators are sometimes interrelated and correlated.

1.2 Description of 4-top $t\bar{t}t\bar{t}$ production

The top quark, t , is the heaviest known fundamental particle, coupling more strongly to the Higgs boson (which gives it its mass) than any other particle. This higher energy level at which the top quark exists leads to large predicted couplings to hypothetical new particles in BSM models, which is why rare processes involving the top quark are so important to study [2]. The processes that are being studied in this analysis, are those where two top quarks, tt , and two antitop quarks, $\bar{t}\bar{t}$, are produced, creating a “four-top,” or $t\bar{t}t\bar{t}$ process. These processes come in many varieties, including interactions with gluons, Higgs bosons, and other fundamental particles. A few examples of Feynman diagrams representing these processes are given below, in *Figure 1*.

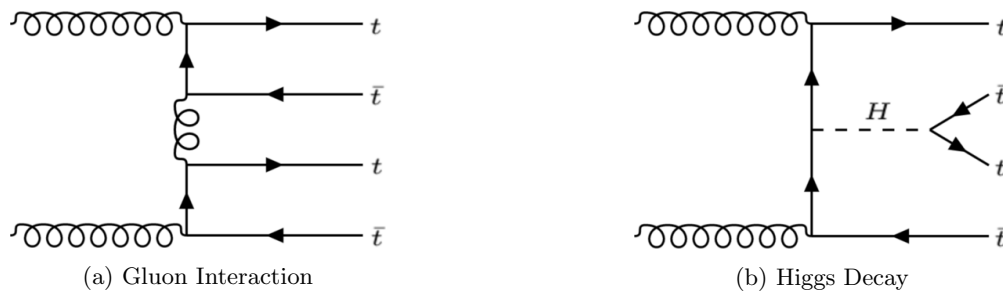


Figure 1: Two common $t\bar{t}t\bar{t}$ production processes that contribute to signal [2]

Within the ATLAS detector, these produced top quarks (almost)¹ always decay into a W^\pm boson and b quark. Then, the W boson either decays leptonically into a lepton and a neutrino, or hadronically into $q\bar{q}'$, while the b -quark turns into a spray or “jet” of fundamental particles seen by the detector. It is these final states which the detector “sees,” and by which the signal is distinguished. As one can imagine, certain other processes with similar final states will produce large amounts of background which must be accounted for. One such example of a large background process with a similar final state is that of $t\bar{t}$ production in association with b jets, as shown below in *Figure 2*. Another complication in separating the $t\bar{t}t\bar{t}$ signal from the background is that neutrinos are essentially invisible to the detector, and can only be deduced to have existed in the detector from the missing transverse energy, \cancel{E}_T , of the collision. Jet multiplicity, jet flavour, event kinematics, as well as other observables are used to separate signal from the background.

This specific analysis looked at four-top production containing *two same-sign leptons, or at least three leptons*, as the alternative *single lepton/opposite-sign lepton pair* signal has backgrounds which are extremely hard to isolate.

1.3 Why is $t\bar{t}t\bar{t}$ useful for EFT interpretations?

There are a few reasons why the $t\bar{t}t\bar{t}$ production process is extremely relevant to study and is ideal for searching for confirmation of BSM models. As mentioned previously, the top quark is predicted to have large

¹almost always because in CKM matrix, the t to b coupling $V_{tb} \approx 0.99$

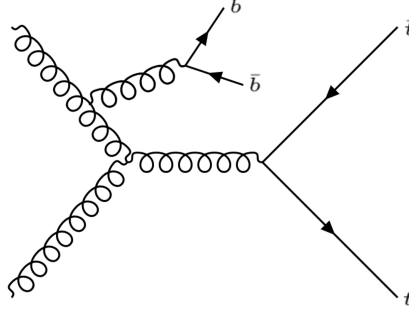


Figure 2: $t\bar{t}$ production, with b -jets, a large background contribution [2]

couplings to hypothetical new particles, which provides many mechanisms by which to increase the cross-section of $t\bar{t}t\bar{t}$ production. These include gluino pair production in supersymmetry theories, scalar gluon pair production, heavy scalar or pseudoscalar boson production with $t\bar{t}$ in type-II 2-Higgs-doublet models, as well as others [2]. Also, the large mass of the top quark implies a large coupling to the SM Higgs boson and, as seen in *Figure 1b*, modifying that coupling will greatly affect the cross-section of $t\bar{t}t\bar{t}$. One such EFT parameter that does this is the Higgs Oblique parameter, \hat{H} , which is the Wilson coefficient of the only dimension-6 operator that modifies the Higgs boson propagator within a Universal EFT: $\mathcal{L}_{\hat{H}} = \frac{\hat{H}}{m_h^2} |D^\mu D_\mu H|^2$ [9]. Modifying the value of the \hat{H} parameter will have a direct impact on the abundance of the Higgs channel four-top production, creating a measurable difference in signal strength from the SM prediction. Other EFT operators which affect the couplings between quark doublets and singlets have similar effects of the production rates of $t\bar{t}t\bar{t}$.

While $t\bar{t}t\bar{t}$ had already been introduced as a worthwhile and relevant candidate for BSM investigation from a theoretical point of view [9], the incentive to research $t\bar{t}t\bar{t}$ experimentally was reinforced by physical observations in a 2021 paper: “Measurement of the $t\bar{t}t\bar{t}$ production cross section in pp collisions at $\sqrt{s} = 13\text{TeV}$ with the ATLAS detector” [2]. The paper measured the four-top production cross-section of events with a single lepton or two opposite-sign leptons, in combination with multiple jets. It also combined the results of this search with the cross-section measured from a 2020 paper [3], where the inclusion criteria were two same-sign leptons, or more than three leptons. Via the combination of these two papers, a signal strength of $\mu = 2.0 \pm 0.4(\text{stat.})_{-0.5}^{+0.7}(\text{syst.}) = 2.0_{-0.6}^{+0.8}$ was measured.² The signal strength, μ , represents the amount of signal measured in relation to the expected amount from the Standard Model ($\mu = 1$ if the SM is true). Although, with uncertainties, the measured μ is only a couple standard deviations away from the SM, the fact that there is any deviation at all is motivation for BSM searches in this realm.

2 Existing Analysis / Tools

Within the EFT part of the overall analysis, these are the tools and programs being used when I started my research. I joined the analysis, working with programs like `trex-fitter` and `mva-trainer`, as well as tools such as Recursive Jigsaw Reconstruction variables and Boosted Decision Tree-made signal regions.

2.1 TRExFitter

TRExFitter is a code framework created for binned profile maximum likelihood fits, and the default fitting tool in the Top Working Group at ATLAS. Its name derives from ‘Top Related Experiment Fitter’ and (unfortunately) has no real relation to the *Tyrannosaurus rex*. It utilises CERN-specific `.root` data files, to fit given signal and background region “template histograms” to data. The data being fit to in

²The *stat.* uncertainties come from the fact that $t\bar{t}t\bar{t}$ production is a rare process, and the *syst.* uncertainties come from the fact that it is a difficult process to measure.

our analyses so far is simply a Monte Carlo (MC) created Asimov data set³, as this analysis is not at the ‘unblinding’ stage yet. TRExFitter is run by a `.config` file in which the different regions, samples, and other configurations of the fit are specified [7].

TRExFitter follows the standard HEP histogram fitting procedures, and this analysis utilizes some new data analysis techniques such as Recursive Jigsaw (RJ) Reconstruction and Boosted Decision Trees (BDTs). Regions are selected to maximize and differentiate signal over background. This is partly done with the variables created from the RJ analysis explained below, which are then fed into the BDT to define a Signal Region within the phase space (which contains at least $< 20\%$ background processes). Adjacent orthogonal regions are then chosen as Control Regions (CRs), and it is in these region where the fitting takes place. Some CRs are created with specific background processes in mind, and try to single them out via phase space cuts. Each different background-specific CR from the MC model samples is then ‘floated’ simultaneously to match the values seen in the data, in our case Asimov. From this, a ‘Normalization Factor’ for each major background is determined via:

$$NF = \frac{N_{data} - N_{other}^{SM}}{N_{bkg}^{SM}} \quad (2)$$

where N_{bkg}^{SM} is for a specific process. In theory, $N_{bkg}^{SM} \cdot NF + N_{other}^{SM}$ should exactly equal N_{data} , however this won’t be the case as many different (and sometimes correlated) CRs and background processes are being fit at once. This is what the fit is optimizing. The normalization factor at which the MC is floated is then applied to the Validation Region(s) (separate from the SR and CRs) to confirm its validity, and the validity of the assumption that the ratios between the MC simulation and the data stay the same between all regions of the phase space. The norm. factors, NF , are then applied to their respective backgrounds within the Signal Region, to determine the signal strength, μ :

$$\mu = \frac{N_{data} - N_{bkg}}{N_{sig}^{SM}} \quad (3)$$

where $N_{bkg} = \sum_i NF_i \cdot N_{bkg_i}^{SM}$, and N_{sig}^{SM} is not scaled, so that $N_{sig}^{SM} \cdot \mu = N_{data} - N_{bkg}$. From this it can be seen that if the Monte Carlo Standard Model Simulation was completely accurate to observed data, μ would be 1.

2.1.1 EFTRExFitter

EFTRExFitter is a modification to the original TRExFitter framework to better allow for the specific functionalities needed for SMEFT interpretation. Spearheaded by the ATLAS TopX Group, specifically the ‘Non-resonant BSM in 4top’ Group, EFTRExFitter was originally implemented by Josh McFayden as an automation to the ‘hacks’ that previous EFT analyses with TRExFitter used [11]. It adds a few new functionalities, including a new sample type ‘EFT SM Reference’ where the simulated ‘EFT Variation Samples’ can be loaded to derive a parametrization of the EFT parameter. In this new sample type, the coefficient of the specific Variation Sample is also inputted. With multiple different coefficient-strength Variation Samples for the same EFT parameter, the new EFTRExFitter can produce ‘QuadFits’ of the effect of the parameter on each separate bin, which are essentially quadratic fits on how different levels (coefficients) of the parameter affect the yield of each bin. These fits are quadratic because the EFT parameters enter into the Lagrangian quadratically. An example of a QuadFit plot can be seen below in *Figure 3*.

2.2 Recursive Jigsaw Reconstruction, RJR

Recursive Jigsaw Reconstruction (RJR) is a method of reconstructing the center-of-mass variables of the collision, from the final-state detector variables. This makes it easier to create intuitive regions for specific variables that are more representative of the physics behind the collision, and not simply just what the detector outputs.

³A range of process-specific MC simulations, using generators tuned for particular processes, are used to simulate all the backgrounds that can enter the process.

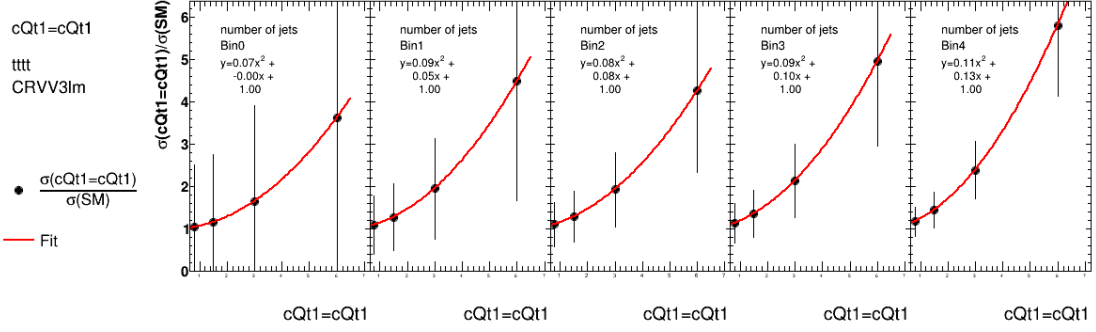


Figure 3: An Example of a QuadFit EFTRExFitter plot, for the EFT parameter $c_{Q_t}^1$ in the 5-bin Control Region VV3lm

RJR uses known physics constraints to reconstruct the kinematics of the collision. These include constraining the invariant mass of the neutrinos to approximately zero— $m_{\nu\nu} \approx 0$, constraining the possible values of the missing energy vector— $\vec{E}_T = (|\vec{p}_T|, \vec{p}_x, \vec{p}_y, \vec{p}_z = 0)$, equating the average angle of visible and invisible final states— $\eta_{\nu\nu} = \eta_{visible}$, and matching the masses of the collision level particles to the top-mass, among many other physics constraints. This allows information (that would otherwise not be directly readable from the detector) such as the momentum of, or the angular spread of the top quarks to be obtained.

Some of the RJ-created variables/regions that I used in this analysis were the following: $\Delta\phi_l^{CM}$, ΔR_{jb}^{CM} , ΔR_{jj}^{CM} , ΔR_{lb}^{CM} , and p_t^{CM} , among others. The CM in these variable names represents the center-of-mass frame of the collision—the frame of the reconstruction. The $\Delta\phi$ and ΔR represent the difference in the angular variables ϕ and R , comparing the objects in the subscript: where l represents a lepton, j represents a hadronic jet and b represents a b-jet specifically. The variable p_t is the momentum of the top quarks. These variables are explained in greater detail in *Appendix B*.

For the MC samples used in this analysis, the RJR versions were accessed by tagging on `_RJR` to the MC file names via a python script named `make_rjr.py`.

2.3 Boosted Decision Trees, BDT

The purpose of the Boosted Decision Tree is to create a Signal Region for the samples via phase space cuts, in essentially asking the question “Is this event background-like or signal-like?” When training the decision tree, it is given the information of whether it is being fed background or signal samples. It then picks a cut value for a particular input variable (in our case, the RJ variables are fed into it) and decides whether that cut differentiates between signal and background or not. The boosted part of this decision tree arises from the fact that it can make refinements to its cuts, and essentially ‘learn’ from how it performs on previous cuts. The BDT maximizes the background-signal distinction with its optimally refined cuts to the phase space, based on the input variables.

The BDT then creates a binary continuum of cuts, ranking them on a scale from -1 to 1, with -1 being the most background-like, and 1 being the most signal-like. In our analysis, this is re-scaled from 0 to 1, with 1, again, being the most signal-like.

2.4 mva-trainer & Graph Neural Networks, GNNs

Later in my work term, the utility of machine learning (ML) algorithms, other than BDTs, on EFT distinction was explored. Specifically, Graph Neural Networks (GNNs) were thought to be the most useful in distinguishing the effects of EFT parameter presence, due to the nature of its representation of the input data.

GNNs are a type of neural network, used for data that can be represented as graphs. This allows for “connection” between the input variables, in a way that correlations and associations are more easily represented. This is useful for EFT analysis, as many EFT parameters are inter-correlated, and shape distinction can be better utilized to train the network. Part of the reason other (non-BDT) ML algorithms were explored is because BDTs tend to wash out minimal shape differences, which is the most useful tool in distinguishing EFT effects. This improvement of GNNs over BDTs is supported by preliminary results from the overall 4-top analysis. From a recent test, “GNN improves 5-10% compared with BDT.” [12]

I used the program `mva-trainer` for the implementation of GNNs in this research. This program is “a framework for the training of deep neural networks and decision trees,” [6] which contains support for multiple different types of neural networks. I worked with Albert Kong, from the University of Adelaide, on the implementation of `mva-trainer` in this 4-top BSM analysis.

3 Procedure / My Contributions

3.1 Working with EFTRExFitter

I have been running EFTRExFitter, as well as the original TRExFitter, with Monte Carlo simulated EFT-varied signals. The EFT Signals (other than \hat{H}) are specific re-weightings of the original MC SM simulation, in the particular way that introducing a specific EFT parameter with a specific coefficient would cause. Right now, only one EFT parameter is varied or introduced at a time, but the sample files also contain combinations of c_{QQ}^1 , c_{Qt}^1 , c_{Qt}^8 , and c_{tt}^1 being varied together. The signal region, defined by the BDT, optimizes the signal of $t\bar{t}t\bar{t}$ containing two same-sign leptons, or 3 or more leptons. Different `.config` files are then run in (EF)TRExFitter, creating fits and producing plots. The program also outputs histogram `.root` files, which contain the yields of the different processes and EFT varied signal.

Using different config files discussed below, I wrote a python script to plot the EFT signal yields, or rates, at different strengths compared to the nominal $t\bar{t}t\bar{t}$ of the given config. Examples of these plots can be seen in *Appendix B*. The Wilson coefficients representing the strengths of each parameter can be seen in the legends of the plots. I also wrote a script normalizing the EFT yields to the “area” of the nominal histogram, for the purpose of comparing shape differences caused by the introduction of certain EFT parameters. For the same parameters as the previous figures, some examples of the shape comparison plots can also be seen in *Appendix B*.

I later modified this script to normalize the nominal yield and EFT-varied yields to an “area” of 1, to quantify the difference in shape with a separation percentage defined by:

$$Sep. = 0.5 \sum \frac{(t - e)^2}{t + e} \times 100\% \quad (4)$$

where t is the normalized nominal $t\bar{t}t\bar{t}$ yield for a given bin, e is the normalized EFT-varied yield for a given bin, and the summation is over all bins in the histogram. This is partly derived from the Kolmogorov-Smirnov Test for probability distribution comparison. As this equation sums over the number of bins, it encodes the importance of bin granularity into the final separation percentage. The values for the separation percentage can be seen at the bottom of the shape comparison plots mentioned above, in *Appendix B*.

3.1.1 Config File Differences

At first, I ran older config files constructed for the original TRExFitter (not the EFT modified version), to get a sense of the functionality of the program. Those configs included all the RJ-variable specific validation regions previously defined for the analysis, however no systematic uncertainties (also called systematics). The config labelled `FourTop.RJ.config` was first run with the Higgs Oblique-modified samples designated as `Type: SIGNAL` as well as the nominal $t\bar{t}t\bar{t}$ Next to Leading Order (NLO) signal. This was however, an incorrect comparison, as the \hat{H} -modified sample was simulated at Leading Order (LO), not NLO. After that was realized, the config was rerun using `“tttt_EFT_default”` as the nominal signal, which was created at

LO and under the same regime as the other EFT variations (excluding \hat{H}). In *Figure 4*, it can be seen that the yield of the nominal signal does indeed change between NLO and LO, confirming that the correct regime matters. At first glance in *Figure 4*, the NLO nominal sample (7a) seems to fit the shape of the Higgs Oblique variation better than the LO *EFT default* nominal (7b) does, however this may just be due to the \hat{H} samples being produced in a different regime, discussed more in section 3.1.2.

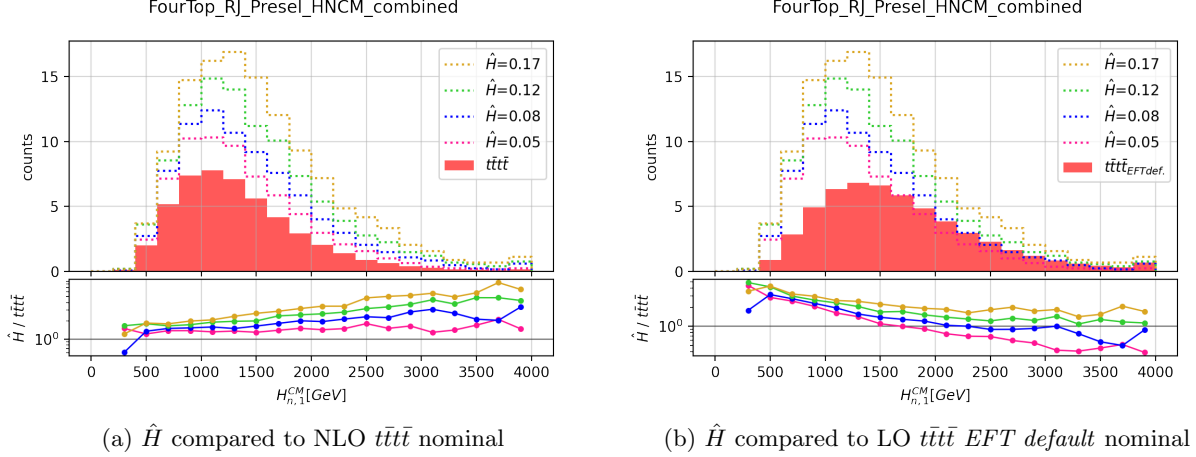


Figure 4: Comparison of difference in nominal yield in the RJ variable region $H_{n,1}^{CM}$

This ‘old’ config was then also run with $c_{Q\bar{Q}}^1$ and $c_{Q_t}^8$ being varied one at a time, as a preliminary shape difference overview, however the yields in the ‘rates’ plots were not appearing as expected. The rates of $t\bar{t}t$, when modified by one of the EFT parameters, were all (or almost all) appearing lower than the nominal rate of the 4-top EFT default LO signal, when the opposite is expected. An example of this can be seen in *Figure 5*, showing the $EFT = 0$ samples far below the nominal. In reality, the EFT samples where the parameter coefficient equals zero should match the rates of the nominal, whereas this was not the case. This was assumed to be due to how the MC EFT samples (excluding \hat{H}) were generated— each EFT-parameter-modified signal sample was not completely regenerated on its own, but is simply a specific reweighting of the nominal 4-top sample. The plot described above was most likely an artefact of an error in reweighting. After this was discovered, an up-to-date ‘replacement’ file was found and used, which specifies the weighting scheme.

After the above steps, the functionalities of *EFTRExFitter* were explored, as it is better suited to EFT analysis. The config files used were based on *EFTRExFitter* config files written by Xiang Chen for related 4-top EFT analyses [5]. After testing out multiple versions of these configuration files, the ones that gave the best results were the files which gave a reweighting to the LO EFT samples to match the ‘regime’ of the NLO nominal $t\bar{t}t$ sample, named with *AppRatio* [5]. In the config-file sample specification for each EFT-varied ‘signal,’ the type was now specified as **Type: EFT**, and the sample block also specified the value of the Wilson coefficient as well as the EFT parameter title and nominal signal reference. The main difference of these configs was their inclusion of **DivideBy: Ref_EFT_LO** and **MultiplyBy: Ref_EFT_NLO**, which essentially ‘reweight’ the LO EFT samples to the nominal NLO regime. In this way, we can still use the higher order NLO samples for the nominal 4-top signal, while being able to compare to LO EFT variations. The **Ref_EFT_LO** and **NLO** references were introduced into the config file as **Ghosts**. This config produced the best results (the $EFT=0$ samples matched the nominal yields as seen in *Figure 6* & all the EFT modified yields are above the nominal sample), and so was used on all the EFT parameters individually: $c_{Q\bar{Q}1}$, c_{Q_t1} , c_{Q_t8} , $c_{t\bar{t}1}$, and \hat{H} . However, as *EFTRExFitter* fits each bin separately, to minimise run-time only a few of the RJ-variable regions were input into the config, again with no systematics.

Plots were created comparing the yields and shapes of different values of each of these parameters, seen in *Appendix B.4*. As these configs were run with *EFTRExFitter*, the previously mentioned *QuadFit* plots were

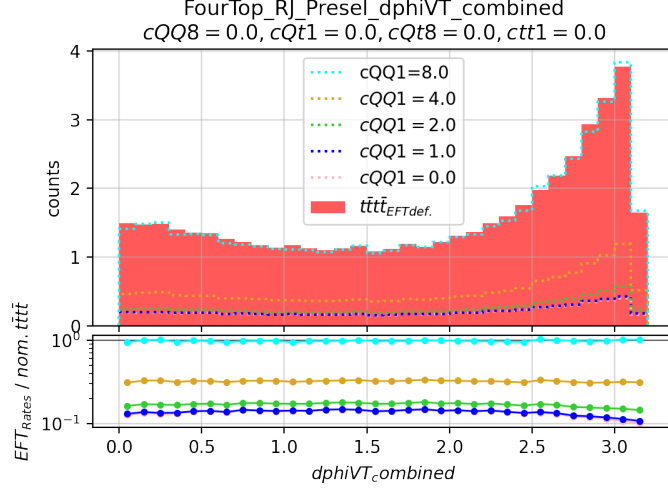


Figure 5: An example of a false re-weighting of EFT-varied signals, causing them to be below the nominal. EFT parameter c_{QQ}^1 is being varied in the RJ variable region ‘ $\Delta\phi_{VT}$ combined’

also created for each RJ-region for each EFT parameter. Later, more RJ-variable regions were added, and the general ‘blanket’ cross-section systematics were added for each of the background and signal samples. This then allowed Negative Log-Likelihood plots to be produced via running the fit, quantifying the Confidence Level of the ‘amount’ of EFT presence in the simulated data. These plots, as well as an uncertainty on the EFT parameter coefficients, can be seen in *Appendix A*. The plots demonstrating yield and shape differences for some of the RJ-variable regions, as well as the QuadFits, can be seen in *Appendix B.4*. A couple new BDT signal regions were also created, to try to improve upon the shape distinction present in the original *SMBDT*. These BDT signal regions can be seen in *Appendix B.1*.

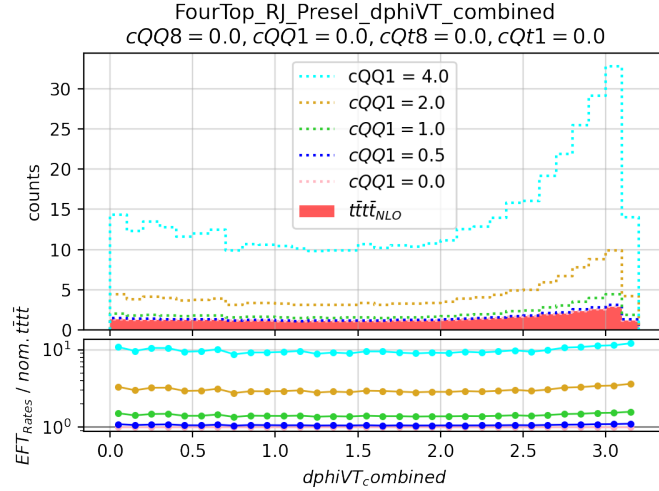


Figure 6: The same region and EFT parameter as *Figure 5*, showing how $c_{QQ}^1 = 0$ now matches the nominal NLO 4-top. This shows the good results from the **AppRatio** configs

While running the QuadFit for the EFT configs, a slight bug in the implementation of EFTRExFitter was discovered. The program quit unexpectedly when it encountered an empty bin, which occurred in some of the RJ-variable Region plots. Abhishek Sharma implemented a fix to this bug using boolean masks.

3.1.2 Higgs Oblique Difficulties

Although the Higgs Oblique samples were generated at LO, as with the nominal *EFT default* samples, they were simulated separately in a different regime. This makes it difficult to compare the \hat{H} rates with either of the nominal $t\bar{t}t\bar{t}$ samples, as seen partly in *Figure 4*. Originally, there were no $\hat{H} = 0$ samples created to act as a nominal signal, however Rachel Lindley, also part of the greater 4-top analysis group, has been working on the comparison of nominal signals and has created an equivalent $\hat{H} = 0$ sample [10]. With the newly created Higgs Oblique nominal, Rachel has been comparing the yields of different detector level output variables with the EFT default nominal LO signal, as well as the NLO SM nominal signal. From her slides, it can be seen that there are slight differences in the three nominal yields, of which the cause is uncertain. She speculates that it might be due to a difference in scale setup. The differences in nominal rates raises questions about whether the analysis is correct in its present form, in comparing the Higgs Oblique samples to the *EFT default* nominal samples *or* the NLO nominal samples. This also means that the shape re-normalization done with the previously discussed **Divide By** is inaccurate, as it divides by the shape of the *EFT def.* LO nominal. Comparison of the Higgs Oblique parameters with the NLO nominal signal can be seen in *Figure 7*, comparing the **DivideBy** renormalization technique and no renormalization. The renormalized plot unexpectedly shows much higher \hat{H} levels, for an unknown reason. Perhaps this indicates that the **AppRatio** renormalization config technique is not suited to \hat{H} in its present form.

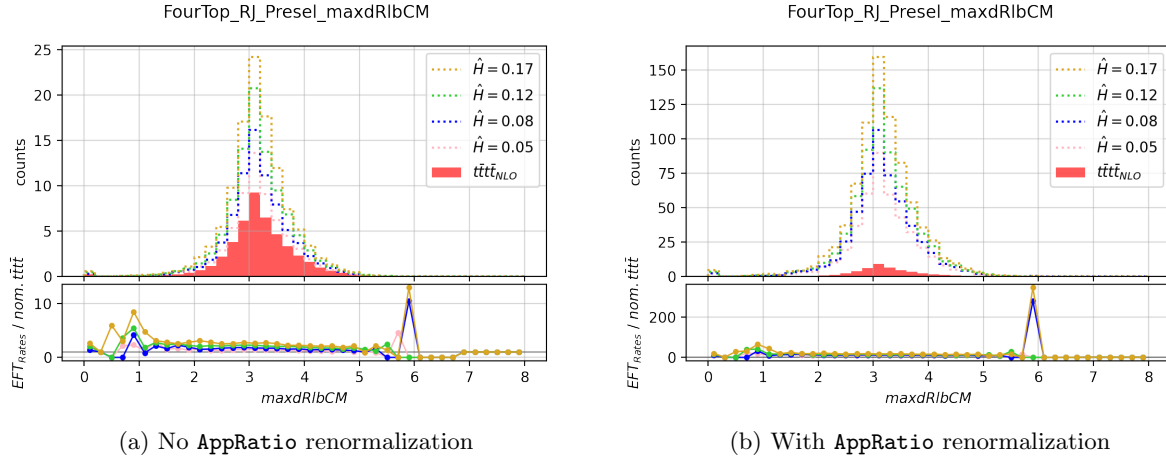


Figure 7: \hat{H} compared to NLO $t\bar{t}t\bar{t}$ nominal, in the RJ variable region $\max\Delta R_{lb}^{CM}$

As of right now, there is no $\hat{H} = 0$ sample able to be used by the rest of the analysis team, and so there is some confusion as to how to go about analysing the Higgs Oblique Samples. To compound the confusion, the QuadFits created by EFTRExFitter for the \hat{H} samples are sporadic and random in their bin-by-bin fitting, as seen in *Figure 8*.

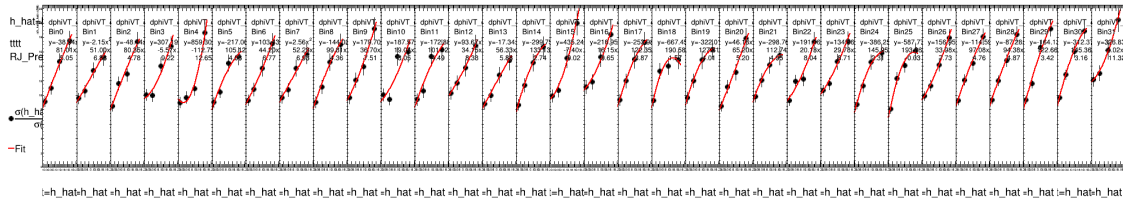


Figure 8: An Example of a the sporadic QuadFit bin-by-bin fitting, for the EFT parameter \hat{H} in the RJ region $\Delta\phi_{VT}$ combined. The badness of the fit can be seen in the inversion in concavity between adjacent bins.

To look into this myself, I made a few plots comparing the NLO nominal $t\bar{t}t\bar{t}$, LO *EFT default* nominal $t\bar{t}t\bar{t}$, and Higgs Obliques $\hat{H} = 0.05, 0.08, 0.12, 0.17$ modified $t\bar{t}t\bar{t}$ signal for some ‘input’ detector level variables (instead of the RJ-created variables used earlier) to assess which nominal is best suited to the Higgs Oblique and to explore the differences in the LO & NLO nominal yields at the detector level. Some of these plots can be seen in *Appendix C*.

3.2 Working with `mva-trainer`

As I started working with `mva-trainer` later in my work term, I did not have the chance to produce much analysis with the program. Working with Albert Kong, `mva-trainer` was set up, all the correct packages were installed (of which there were many), and some test configuration files were run to explore the functionality of the program.

I was able to run the conversion script on the analysis samples, which converts the file type from `.root` to `.hdf5` files, which can more easily be handled by the python libraries which `mva-trainer` is built upon.

Unfortunately, there was not much progress beyond this as the GNN implementation of `mva-trainer` is still under development. I familiarized with the program but was unable to train on any data, or fully explore the GNN utilities of `mva-trainer`. Hopefully the GNN sector of this program will be ready for use soon, but it was not available by the time my work term ended.

4 Results / Discussion

4.1 Findings & Results

Many yield and shape comparison plots were created in the RJ-variable regions, as well as in some Signal Region(s), Control Regions, and Validation Regions, seen in *Appendix B*. After some minimal systematics were introduced, Negative Log-Likelihood plots were also created, quantifying the confidence levels of the existence of the analyzed EFT parameters, at different coefficients. These are seen in *Appendix A*. Comparisons of the different nominal $t\bar{t}t\bar{t}$ signal samples (Leading Order and Next to Leading Order) and the \hat{H} varied samples, for the input variables, were plotted in *Appendix C*.

Although my research was mostly of an exploratory nature, it was found that the RJ-variable regions containing information on top quark momentum had the largest shape differences and are therefore the best (of the variables tested) at distinguishing EFT effects. This is seen in the *topP_combined* variables in *Appendix B.4*, and in the high values of the separation quantification described in *Equation (4)*.

It can also be seen, in *Appendix B.1*, that the new BDT signal regions did not improve shape distinction much from the original SMBDT, but still had some minimal improvement.

In *Appendix A*, the Negative Log-Likelihood (NLL) plots show different Confidence Levels for the same levels of different EFT parameters (notice the different scales on the x-axis). The NLL value represents the number of sigma deviations from the measured value. A Confidence Level (CL) percentage can be assigned to the NLL value. A NLL of 1 corresponds to a CL of 68%, and a NLL of 2 corresponds to a CL of 95%. Different values of each parameter, at 95% confidence level can be seen in *Appendix A*.

From *Appendix C*, it can be seen that the shape of the \hat{H} samples’ distribution seems to match that of the nominal $t\bar{t}t\bar{t}$ at Next to Leading Order (NLO), rather than Leading Order (LO), even though the \hat{H} samples were supposedly produced at LO.

4.2 Future Directions / Discussion

It is interesting to see that the introduction of EFT parameters seems to most greatly affect the momentum of the top quarks, skewing them to higher values. A potential reason for this phenomenon is the fact that EFT parameters play a larger role at higher energies, and so it would make sense that when introduced, they would cause more higher energy interactions as they are contributing to the physics of the collision. The fact that the NLL plots are so different from parameter to parameter, is an interesting characterization

of the effects of each parameter. The fact that they are so disparate is unusual and may point to some missing systematics, unaccounted-for effects in the simulations, or even actual physical phenomena, perhaps caused by the correlation of parameters. Also, in *Appendix C*, the fact that the \hat{H} seem to better match the NLO nominal samples raises the question of which nominal sample to use with \hat{H} , and if there may be errors unaccounted for in the \hat{H} samples, or if perhaps there are physical phenomena present in the activation of the \hat{H} parameter which are not being accounted for.

For future continuation of analyses in this realm, many different possible paths could be continued and studied. One could start combining the RJ variables to create new variables, perhaps finding a combination that even better separates EFT effects than the $topP$ variables. A combination of the momentum variables, and kinematic spatial variables might perform better than either alone. Working toward a larger shape difference between the nominal and EFT samples is useful because it provides a concrete difference on which a Machine Learning algorithm can be trained to distinguish. As BDTs tend to wash out minimal shape differences, GNNs will most likely perform better at this distinction. Future continuation of this analysis would provide concrete evidence for this. Continuing with GNNs, the algorithm could hopefully be trained to predict the presence different Wilson coefficient levels, as a regression algorithm, rather than simply classification of EFT or no-EFT.

The anomalies with the Higgs samples could be explored more, by creating a $\hat{H} = 0$ nominal sample, as well as samples with higher statistics. Further exploration could also include the addition of more systematics and the activation of many parameters at once, which would help quantify the correlation of the EFT parameters.

References

- [1] Asbah, Nedaa-Alexandra et al.: ATLAS Collaboration (Unpublished as of 2022). *Measurement of $t\bar{t}t\bar{t}$ Standard Model Production and Search for non Resonant New Physics in the Multilepton Final State in Proton-Proton Collisions with the ATLAS Detector*. CERN, internal note.
<https://cds.cern.ch/record/2765538?>
- [2] ATLAS Collaboration (2021). *Measurement of the $t\bar{t}t\bar{t}$ production cross section in pp collisions at $\sqrt{s} = 13\text{TeV}$ with the ATLAS detector*. CERN, report.
<https://atlas.web.cern.ch/Atlas/GROUPS/PHYSICS/PAPERS/TOPQ-2020-10/>
- [3] ATLAS Collaboration (2020). *Evidence for $t\bar{t}t\bar{t}$ production in the multilepton final state in proton-proton collisions at $\sqrt{s} = 13\text{TeV}$ with the ATLAS detector*. CERN, report.
<https://atlas.web.cern.ch/Atlas/GROUPS/PHYSICS/PAPERS/TOPQ-2018-05/>
- [4] Brivio, Ilaria et al. (2019). *O new physics, where art thou? A global search in the top sector*. JHEP, report.
<https://arxiv.org/abs/1910.03606>
- [5] Chen, Xiang (2022). *TopPlusX configs*. Git repository.
https://gitlab.cern.ch/atlasphys-top/TopPlusX/4tops/4top_final_fit/-/tree/EFT
- [6] *Documentation for mva-trainer*. GitLab, documentation website.
<https://mva-trainer-docs-site.docs.cern.ch/>
- [7] *Documentation for TRExFitter*. GitLab, documentation website.
<https://trexfitter-docs.web.cern.ch>
- [8] Ellis, John (2021). *SMEFT Constraints on New Physics Beyond the Standard Model*. BSM-2021 Conference, Zewail City, Egypt.
<https://arxiv.org/abs/2105.14942>

- [9] Englert, Christoph (2019). *The \hat{H} -Parameter: An Oblique Higgs View*. JHEP, report.
<https://arxiv.org/abs/1903.07725>
- [10] Lindley, Rachel (2022, Jun 1). *Kinematic Comparison of Higgs Oblique Samples*. TopX WG, meeting presentation slides.
https://indico.cern.ch/event/1155812/contributions/4919568/attachments/2461310/4219954/Kinematic_Comparison_Rivet_2022.06.13.pdf
- [11] McFayden, Josh (2021). *EFTRExFitter*. CERN, meeting presentation slides.
https://indico.cern.ch/event/1095243/contributions/4607340/attachments/2346122/4000735/2021-11-15_EFTREx_4tops_mcfayden.pdf
- [12] Tsai, Meng-Ju et al. (2022, Aug 15) *Four Top EFT Update with EFTREx-Fitter*. TopX, WG, meeting presentation slides.
https://indico.cern.ch/event/1182461/contributions/5004536/attachments/2493114/4281519/Four_Top_EFT%20Update_With_EFTrex-fitter_220815.pdf

A Appendix: Negative Log-Likelihood Plots

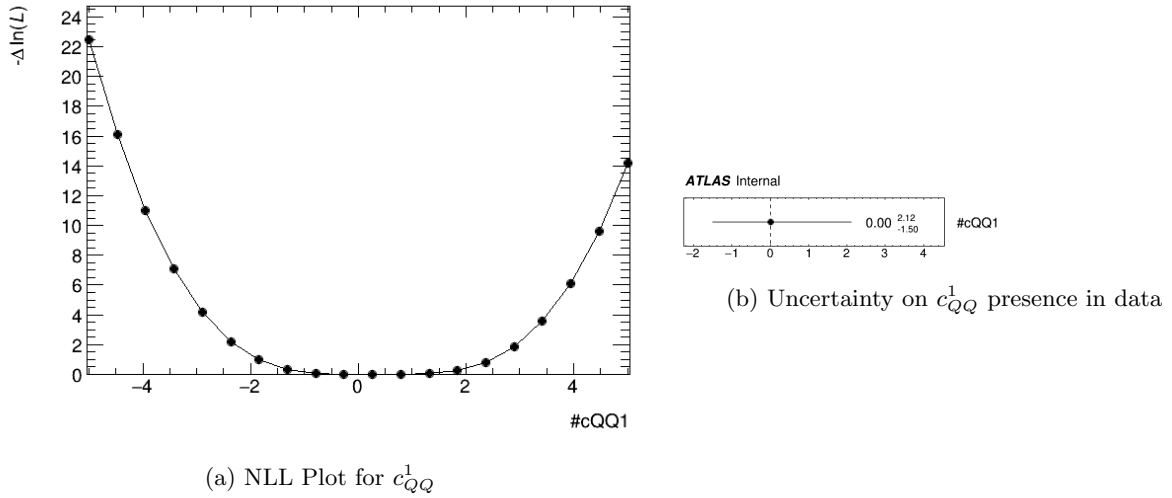
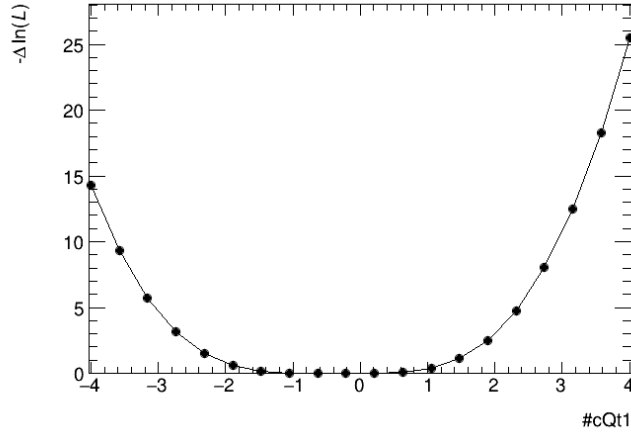
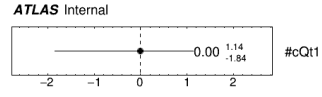


Figure 9: Fit Results for c_{QQ}^1

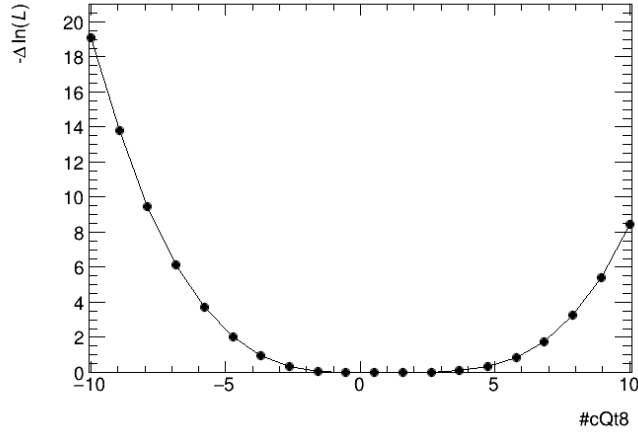


(a) NLL Plot for c_{Qt}^1

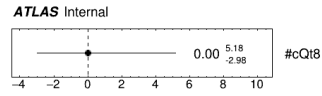


(b) Uncertainty on c_{Qt}^1 presence in data

Figure 10: Fit Results for c_{Qt}^1

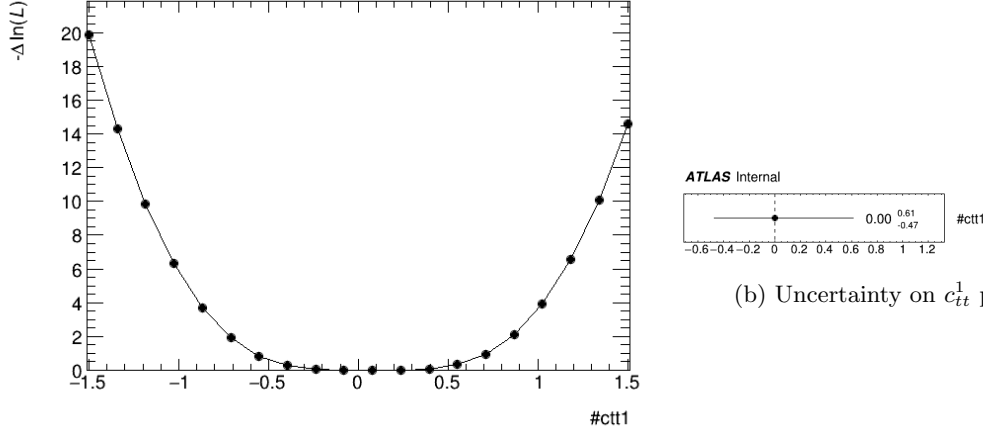


(a) NLL Plot for c_{Qt}^8



(b) Uncertainty on c_{Qt}^8 presence in data

Figure 11: Fit Results for c_{Qt}^8



(a) NLL Plot for c_{tt}^1

Figure 12: Fit Results for c_{tt}^1

B Appendix: Rate and Shape Comparison Plots

B.1 Signal Region(s)

The original Signal Region, *SMBDT*, was slightly modified to see if better shape difference could be achieved. The BDT was run again, resulting in the new signal regions *BDT_RJ* and *BDT_RJ2*

SMBDT

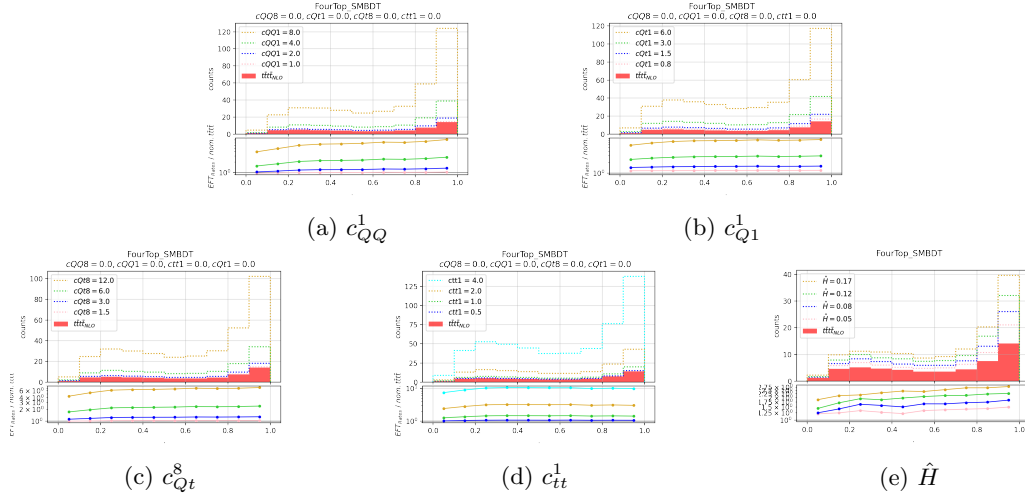


Figure 13: Yield / Rate comparisons in the SMBDT Signal Region, for all the tested parameters

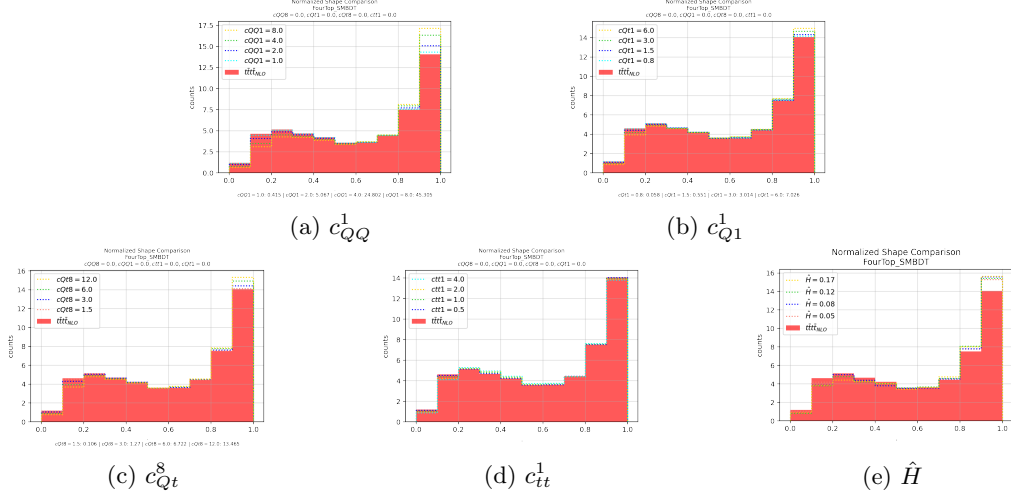


Figure 14: Shape comparisons in the SMBDT Signal Region, for all the tested parameters

BDT_RJ

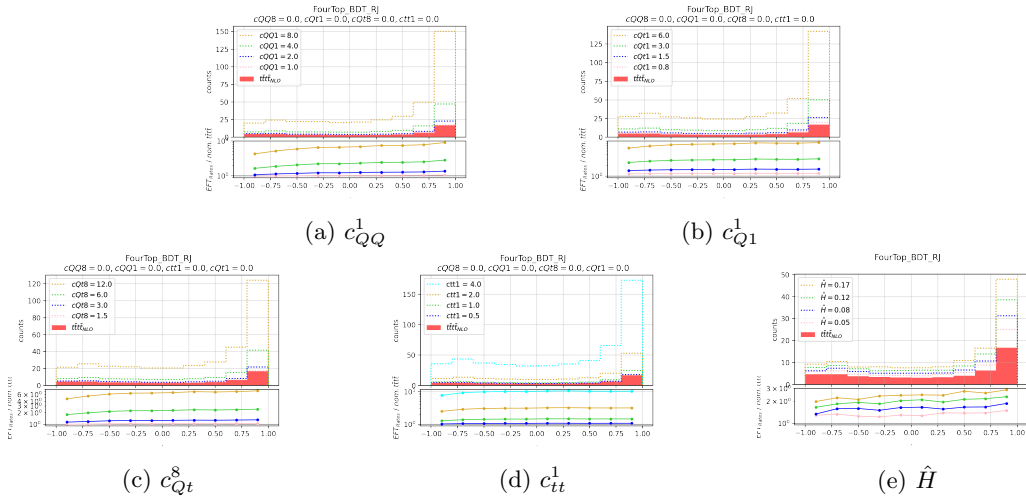


Figure 15: Yield / Rate comparisons in the BDT_RJ Signal Region, for all the tested parameters

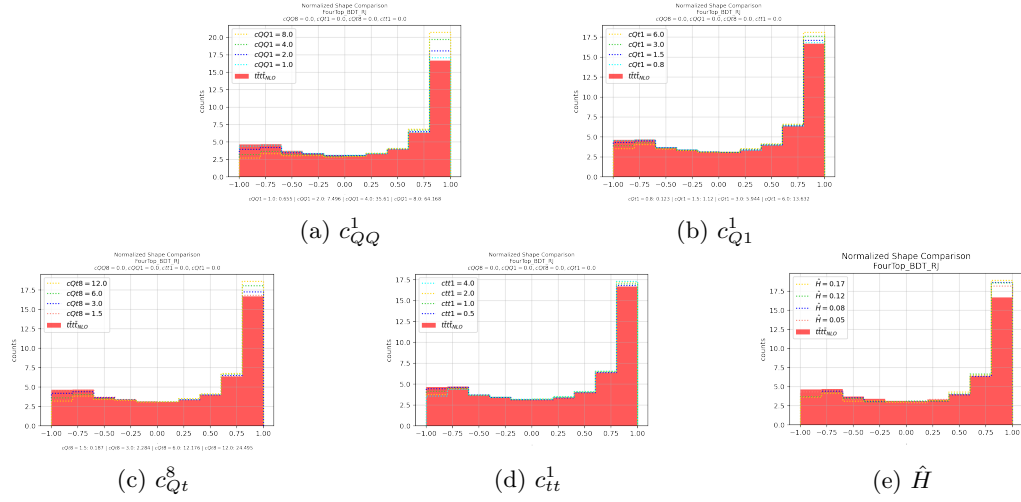


Figure 16: Shape comparisons in the BDT_RJ Signal Region, for all the tested parameters

BDT_RJ2

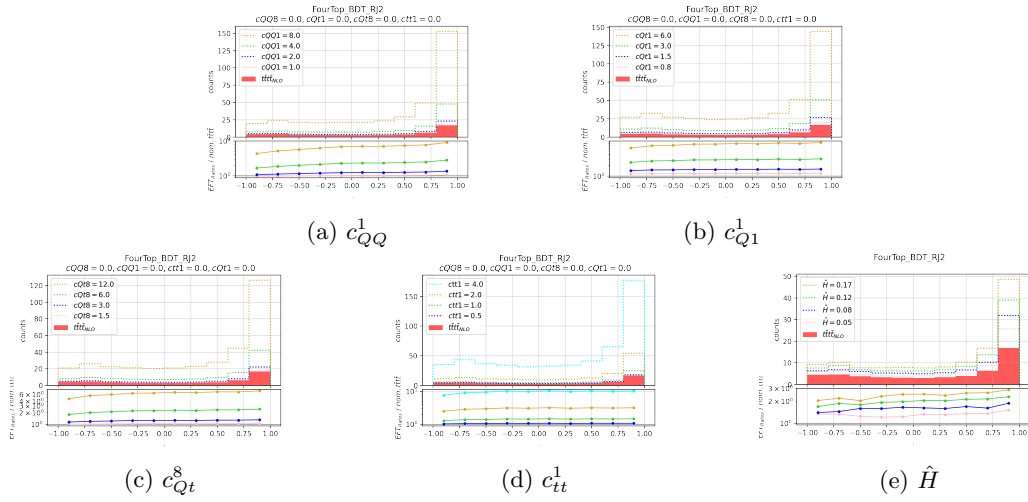


Figure 17: Yield / Rate comparisons in the BDT_RJ2 Signal Region, for all the tested parameters

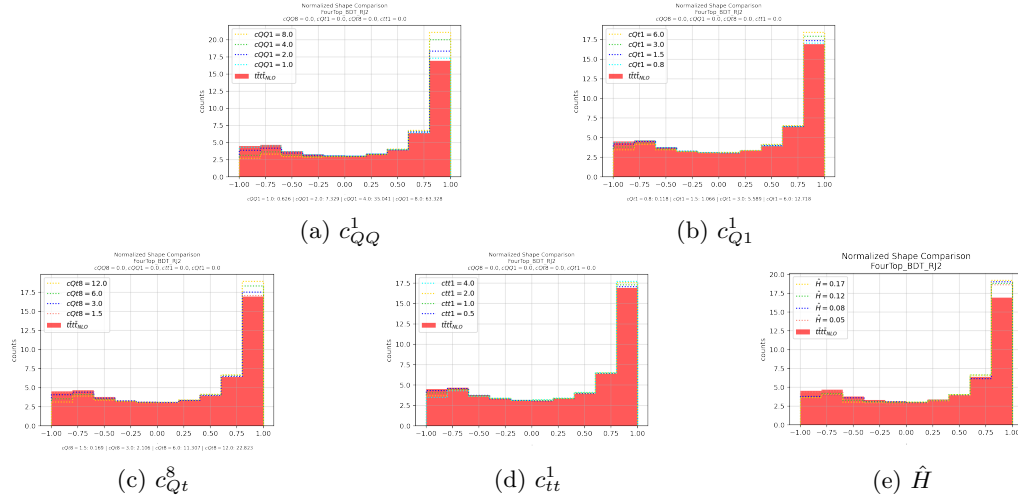


Figure 18: Shape comparisons in the BDT_RJ2 Signal Region, for all the tested parameters

B.2 Control Regions

Note: to reduce the size of the appendix, some figures can be found online at the following link:
<https://bit.ly/3qxs05D>

The Control Regions, adjacent yet orthogonal to the signal region, are used in the fitting process, as explained in section 2.1. Here are a couple examples of the effect of the EFT parameters in the CRs.

- **CRLowBDT**: This is the Background-Like phase space selection from the trained BDT, putting an extra constraint on the fitting.
- **CRttW2l_new**: This is the region isolating the ttW production with 2 leptons in the final state, a major background for $t\bar{t}t$ production.

B.3 Verification Regions

I have only included one example of a “VR” verification region here because the RJ Reconstructed variable regions, seen below, we’re also used as verification regions. Verification Regions do not affect the fitting process.

- **VRttZ3l**: This region represents the part of the phase space corresponding to the ttZ to $3l$ background.

B.4 Recursive Jigsaw Regions

These are a few examples of the RJR regions. The variables represented are described in their respective section.

HT angle combined

The variable *min HT angle* describes the minimum angle $\Delta\phi$ between any two top quark vectors in the CM frame.

R_HTN_HN - $H_{n,l}^{CM}$

This variable represents the transverse sum of object momenta divided by the full sum of the object momenta.

dphiVT - $\Delta\phi_{VT}$

This variable represents the angle, $\Delta\phi$ between the first top quark candidate and the rest of the visible products in the CM frame

dphilCM - $\Delta\phi_l^{CM}$

This variable represents the $\Delta\phi$ between two leptons in the center-of-mass frame

dRjbCM - ΔR_{jb}^{CM}

This variable represents the ΔR between a jet and b-jet in the center-of-mass frame. Both $\min\Delta R_{jb}^{CM}$ and $\max\Delta R_{jb}^{CM}$ are shown

dRjjCM - ΔR_{jj}^{CM}

This variable represents the ΔR between two jets in the center-of-mass frame. Both $\min\Delta R_{jj}^{CM}$ and $\max\Delta R_{jj}^{CM}$ are shown

dRlbCM - ΔR_{lb}^{CM}

This variable represents the ΔR between a lepton and a b-jet in the center-of-mass frame. Both $\min\Delta R_{lb}^{CM}$ and $\max\Delta R_{lb}^{CM}$ are shown.

topP - p_t^{CM}

This variable represents the momentum of the top quarks in the center-of-mass frame. Here $\min p_t$, $\max p_t$, and Σp_t are shown. These variable had the highest shape difference out of any other variables.

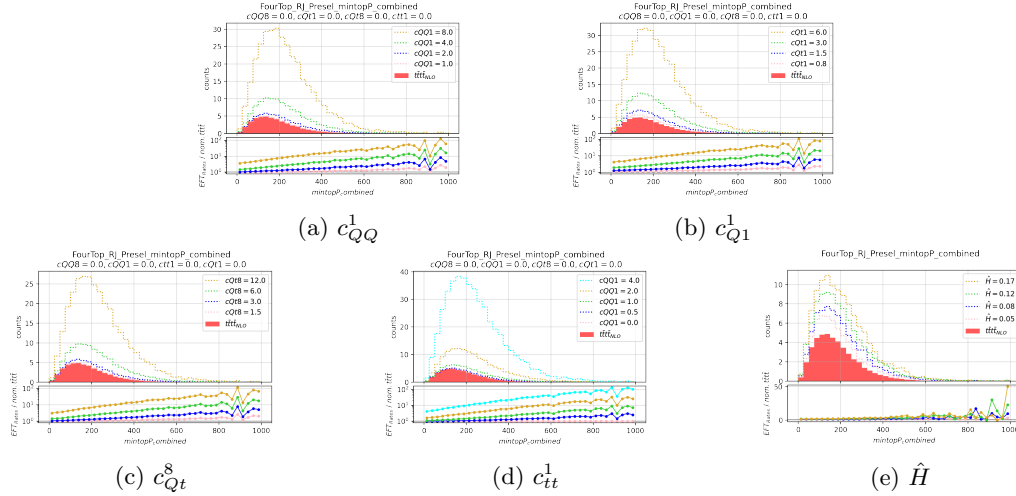


Figure 19: Yield / Rate comparisons for the variable $\min p_t$

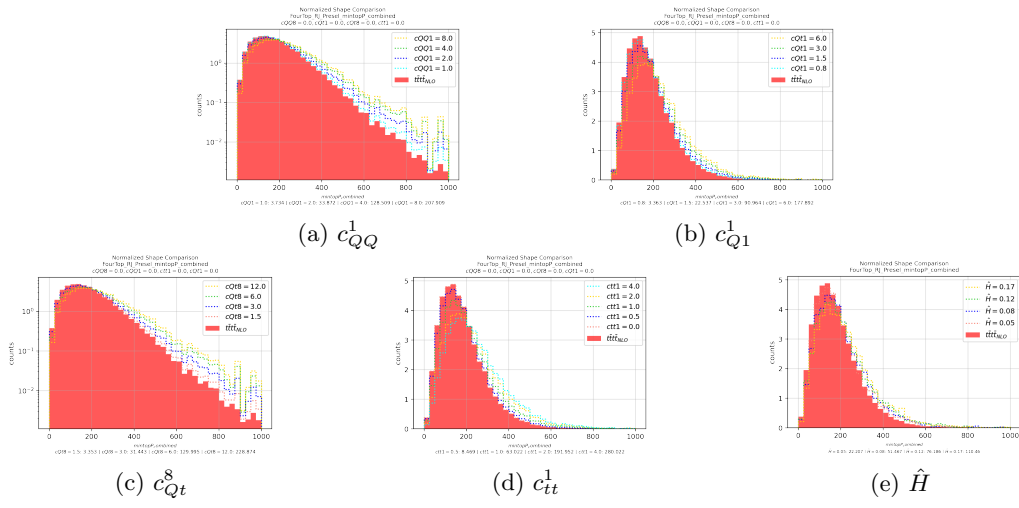


Figure 20: Shape comparisons for the variable $\min p_t$, showing the high values for the shape difference test. The y-axis is sometimes log-scaled.

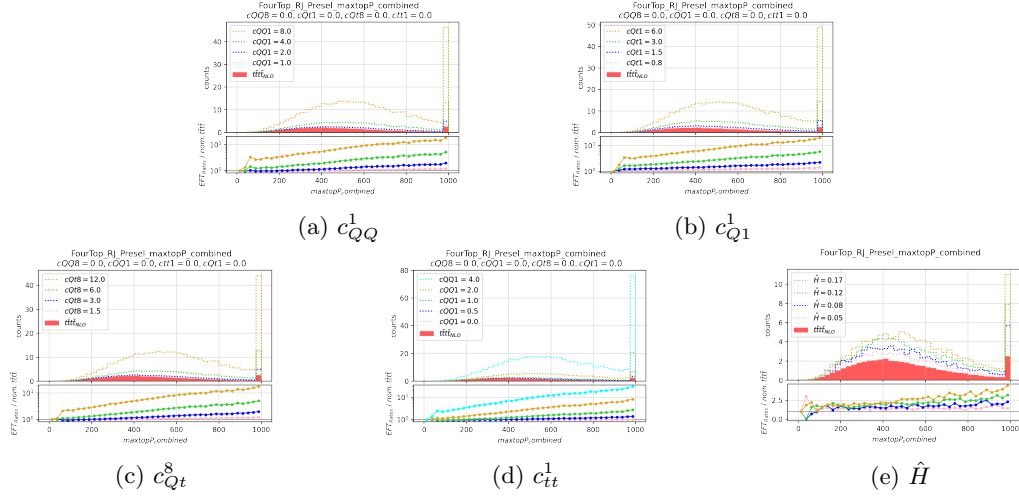


Figure 21: Yield / Rate comparisons for the variable $\max p_t$

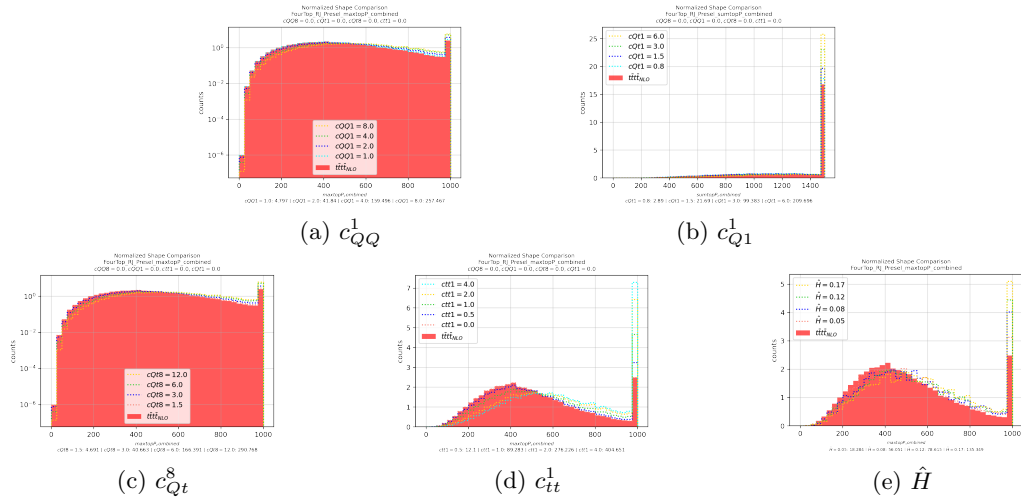


Figure 22: Shape comparisons for the variable $\max p_t$, showing the high values for the shape difference test. The y-axis is sometimes log-scaled.

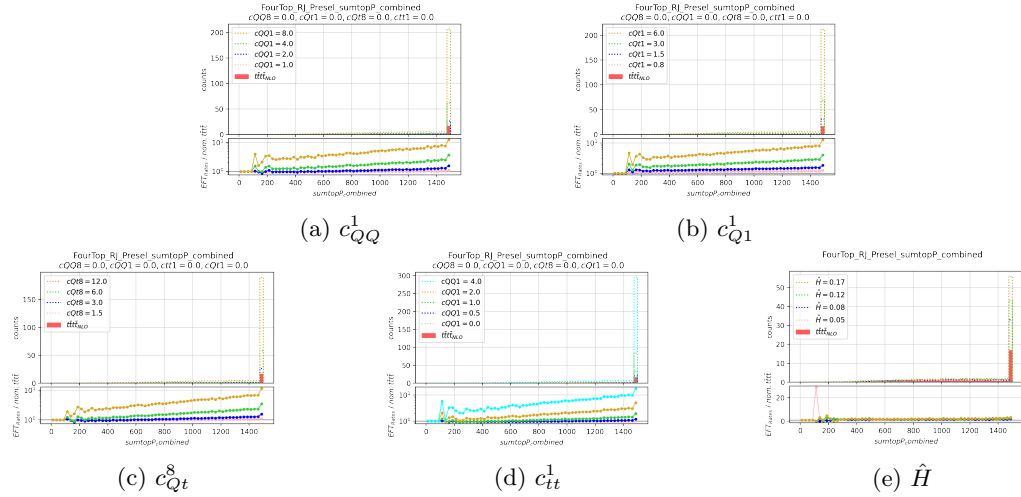


Figure 23: Yield / Rate comparisons for the variable Σp_t . This region should be rebinned for clearer analysis

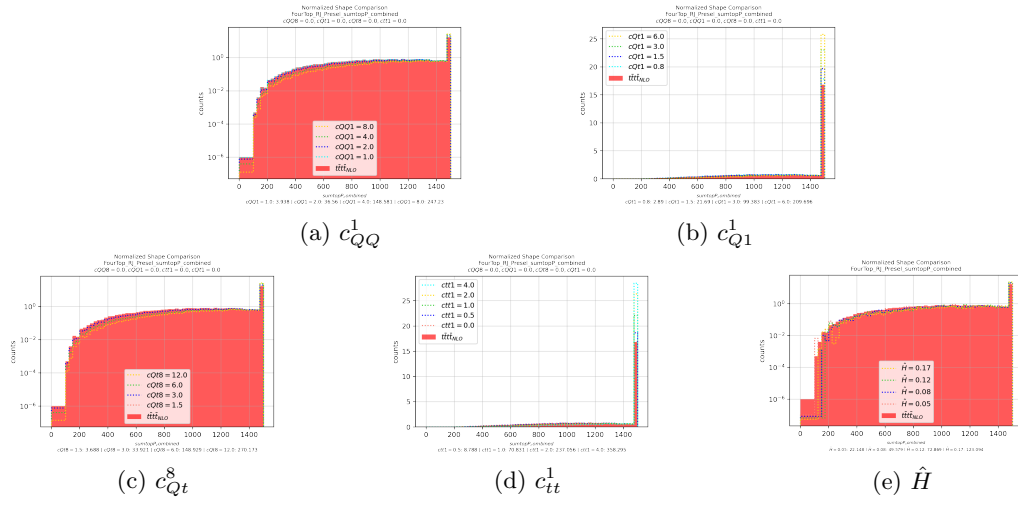


Figure 24: Shape comparisons for the variable Σp_t , showing the high values for the shape difference test. The y-axis is sometimes log-scaled.

C Input Variables for \hat{H} and Nominal $t\bar{t}t\bar{t}$ Comparison

Note: to reduce the size of the appendix, some figures can be found online at the following link:
<https://bit.ly/3qxs05D>

These are the comparison plots between the LO nominal, NLO nominal, and \hat{H} modified signal samples, for the detector level input variables.